Osmers, Jan ; Kaiser, Nils ; Sorg, Michael ; Fischer, Andreas

Adaptive finite element eye model for the compensation of biometric influences on acoustic tonometry

Journal Article	as:	peer-reviewed accepted version (Postprint)
DOI of this document*(secondary publication):		https://doi.org/10.26092/elib/3329
Publication date of this document:		20/09/2024

* for better findability or for reliable citation

Recommended Citation (primary publication/Version of Record) incl. DOI:

Jan Osmers, Nils Kaiser, Michael Sorg, Andreas Fischer,
Adaptive finite element eye model for the compensation of biometric influences on acoustic tonometry,
Computer Methods and Programs in Biomedicine, Volume 200, 2021, 105930, ISSN 0169-2607,
https://doi.org/10.1016/j.cmpb.2021.105930.

Adaptive finite element eye model for the compensation of biometric influences on acoustic tonometry

Jan Osmers*, Nils Kaiser, Michael Sorg, Andreas Fischer

University of Bremen, Bremen Institute for Metrology, Automation and Quality Science (BIMAQ), Linzer Str. 13, Bremen 28359, Germany

Keywords:
Corneal vibration
Transient simulation
FEM
Eye model
Intraocular pressure
Glaucoma

1. Introduction

Glaucoma is causative for 8 % of world cases of blindness [1]. Currently there is no medical method to cure glaucoma, which makes the disease the major reason for irreversible blindness worldwide [2]. The medical intervention is aimed at maintaining vision by reduction of the intraocular pressure (IOP). With a reduced IOP, the mechanical stress to the optic disc decreases and the neural ganglion cells are supposed to receive an improvement in nutrient supply by the arterial system [3]. An early diagnosis and a gentle and precise determination of the IOP are crucial for an effective therapy of glaucoma [4].

According to the current state of the art, all known measurement methods for measuring the IOP have a dependence of the measured value on the eye geometry [5,6]. The Goldmann applanation tonometer (GAT) is the gold standard for tonometry for years. It determines the IOP from the force required to flatten the cornea with a glass stamp [7]. In a variety of studies it was found, that the GAT measurement result has cross-sensitivities to the corneal curvature and thickness [6,8,9]. In order to compensate for the influence of the corneal thickness on the GAT measurement there is the so-called Dresden correction table [8]. Thus proceeding from the average value of the central corneal thickness d from 550 µm, 1 mmHg adds when d decreases by 25 µm, and 1 mmHg subtracts when d increases by 25 µm [8,10]. The background of this correction is the cross-sensitivity with respect to d as biometric eye parameter. Due to the different resistance of the structure to the GAT measuring head, a cornea of below-average thickness leads to

* Corresponding author.
E-mail address: j.osmers@bimaq.de (J. Osmers).

an IOP measurement value that is too small or an above-average thickness of the cornea leads to an excessive IOP reading. In the comparative study “Ocular Hypertension Treatment Study (OHTS)” it was found in glaucoma patients that those with a thinner *d*, related to the comparison group with thicker *d*, showed a stronger degeneration of neural ganglion cells [9,11]. In this context, there is the thesis that inadequate medication was used in patients due to the often underestimated IOP values and thus an insufficient reduction of the IOP was significantly disadvantageous for the disease's progression. Besides influences of biometric eye parameters, the GAT measurement requires anesthesia and etching of the cornea that irritates the tissue and hence the GAT is limited for acquisition of diurnal IOP fluctuations.

Besides the GAT, air pulse tonometers are broadly used to determine the IOP. The measurement principle is based on an air jet that flattens the cornea. The time that passes for the applanation of the cornea is measured and led back to the IOP. The measurement principle also depends on the biomechanical properties of the cornea. With the *Ocular Response Analyzer (ORA)* from *Reichert*, the *Corvis ST* from *Oculus* and the *VX120* from *Visionix* there are already three air pulse tonometers which take biomechanical properties of the cornea into account in IOP measurement and calculate a biomechanically corrected IOP value [5,12]. The *ORA* also detects the second state of corneal applanation by the air jet, which occurs, when the cornea flips back from a temporarily concave shape. The software of the *ORA* then calculates the corneal hysteresis of the two applanation states, that is independent from the IOP [13]. The corneal hysteresis can be used to implement biomechanical influences of the cornea in the determined IOP value. Despite the IOP correction, the *ORA* has no reduced measurement uncertainty compared to common air pulse tonometers without correction [14]. Joda et al. [15] developed a correction formula for the *Corvis*, that is probably used in a similar form in the *Corvis ST*. It was created by using a finite element model in the software Abaqus, that models the cornea, sclera and the inner liquids of the eye. The parameters *d* and *age* were found to be dominant and are consequently used in the final correction formula [15]. For the *Corvis ST*, the measurement uncertainty was reduced by the correction formula and the influence of *d* is compensated [16]. The *Visionix VX120* is a combination of devices that measure IOP, pachymetry (*d*), corneal topography and aberrometry. Therefore it can use several parameters to calculate a biomechanically corrected IOP. Briceno et al. [17] have shown for the *VX120*, that the influence of *d* according to the Ehlers equation [18] can also overcompensate cross sensitivities, which leads to an increase of measurement deviations. There will come up more devices that are a combination of measurement instruments for biometric eye parameters and IOP, which allow to calculate biomechanically corrected IOPs.

Nevertheless, the mechanical deformation and stress of the cornea during measurement with an air pulse tonometer is high and measurement deviations can occur due to the patient's defense reactions.

For this reason, a gentle self-tonometer was realized, with which the patient can determine diurnal IOP fluctuations independently at home [19]. The acoustic measuring approach used for the self-tonometer works with a gentle acoustic oscillation excitation of the eye. The loudspeaker forms a coupled system with the gas volume in the pressure chamber and the connected eye. The loudspeaker's membrane oscillation is detected by a reflection sensor, see Fig. 1. The damping of the speaker's membrane after system excitation is initially found to be sensitive to the IOP of the connected eye.

The amplitude of the excited corneal deflection is a further sensitive parameter for measuring the IOP [20]. The amplitude of the corneal deflection can be measured directly with an optical sensor. Despite the low deformation of the cornea of less than 200 µm,

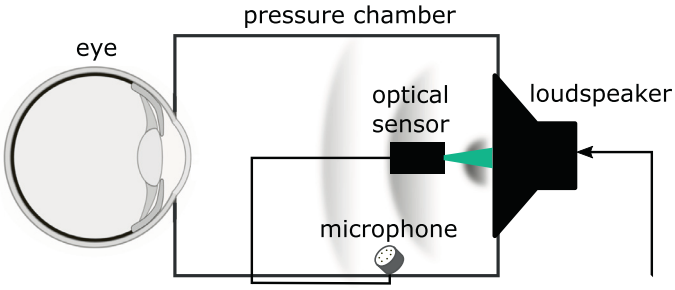

Fig. 1. Principle of the acoustic tonometer.

however, the measurement result has shown to depend on the biometric eye parameters, as in other established tonometry methods. Since several biometric parameters change simultaneously in different real eyes, it is not feasible to perform a statistical analysis from laboratory experiments, to investigate discrete influences of single biometric eye parameters. A large amount of eyes would be needed to allow for significant results for various eye parameters. For this reason, a model-based approach to investigate the influence of biometric variations of the eye on the IOP measurement with the acoustic tonometry principle is required.

There have been several finite element models of the human eye with a broad variation of applications. Concerning acoustic tonometry Coquart [21] has developed a comparably simple model with finite element method (FEM) to investigate the shift of eigen values as a function of the IOP. Coquart has not validated his results or considered to analyze the influence of biometric eye parameters. The influence of a geometrical variation of the eye was investigated by Drescher [22]. He used an eye model from shell elements representing sclera and cornea similar to [21] and additionally modeled the inner fluid. Drescher [22] demonstrated the influence of geometrical changes on the eigen values. A validation was performed with a silicon globe.

Salimi et al. [23] developed a more complex eye model with fluid-structure interaction (FSI) and showed the IOP-dependent frequency shifts of the eigen values. The shell based model represented cornea, sclera, lens and ciliar body to hold the lens. Salimi et al. [23] validated a simplified version of his model with experimental modal analysis on a rubber ball. According to Salimi et al. [23] the influence of biometric eye parameters in acoustic tonometry is smaller than with GAT.

Nejad et al. [24] list in their review the manifold applications of FEM simulations of the cornea. They explain that the focus of the simulation depends on the specific research question, i.e. fiber-matrix composites were simulated in order to take into account the microstructure of the corneal cells in the simulation [25–27]. Most recent simulations however implement non-linear material behavior of the cornea such as Neo–Hooke, Mooney–Rivlin or Ogden material models [28] in the FEM program. When the whole eye is modeled, simplifications concerning the microstructure must be made in a targeted manner so that the simulation can be carried out with the available computing power.

Karimi et al. [29] have used an FSI simulation to investigate damage effects of a pressure wave caused by an explosion or different blunt objects, such as tennis balls on the eye [30]. In doing so, they have recreated the eye in great detail with all major eye components and the eye environment, consisting of muscles and fat tissue. In addition, the simulation model was also used to determine the existing stress and strain in the individual eye components at three IOP levels [31]. The determination of biometric influences on an IOP measurement principle was not described by Karimi et al. [29,31] and a validation of the simulation results was not performed.

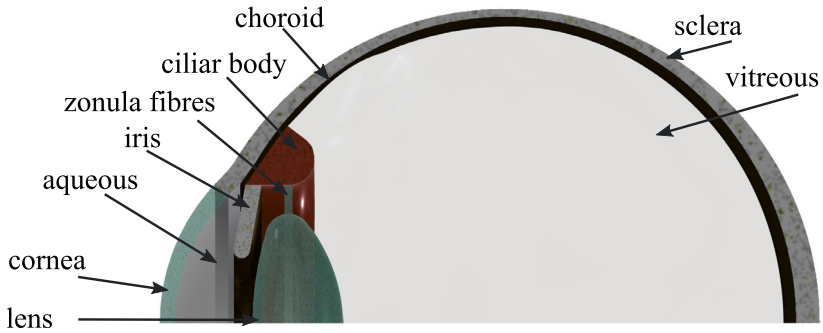

Fig. 2. Components of the parameterizable geometric eye model as CAD construction.

Summarizing the current state of the art, there are different approaches for modeling eye vibrations, also for checking acoustic tonometry approaches [21–23] with varying degrees of detail. However, non of the developed eye models is usable for the parameterized analysis of systematic uncertainty contributions resulting from biometric eye parameters for the acoustic self-tonometer.

In order to allow for quantification of the influence of discrete biometric eye parameters on the corneal deflection amplitude, an adaptive finite element eye model is created and described in this journal contribution. In Section 2, the adaptive eye model is presented with which the biometric eye parameters can be varied in the physiological range and their effect on the oscillation amplitude of the cornea can be calculated. This is followed by the description of laboratory setup for porcine eye measurements. Then, in Section 3, the results of the validation measurements are presented along with the model predictions. The contribution of the model predicted systematic influences of two sample biometric parameters (central corneal thickness and axial length of the eye) on the measurement uncertainty of the IOP determination is then derived from the eye model. In Section 4 the simplifications of the eye model and the results achieved therewith are discussed and in Section 5 finally the article is summarized and an outlook is given.

2. Methods

2.1. Adaptive finite element eye model

The adaptive finite element eye model consists of an eye geometry generated in a Computer Aided Design (CAD) software and a simulation environment represented by the FEM software *ANSYS Workbench 19.1*. Within the simulation environment the imported CAD geometry is assigned with material parameters and boundary conditions. The eye components are then meshed to allow for discrete computation of the occurring forces and displacements to the geometry. Therefore a transient simulation module is used, since the problem of the simulation has to be considered time-resolved due to the dynamic measuring principle of the acoustic self-tonometer.

2.1.1. Design considerations

The eye model is designed in the CAD system with the aim of adjustability that allows the user to adapt the construction to any physiologically possible eye shape and quantify the deviations to the average shaped eye concerning the corneal deflection. Fig. 2 shows the structure and the main components of the eye model, which is available as parameterizable CAD geometry. The model is limited to the macrostructure of the eye consisting of cornea, sclera, zonula fibres, ciliar body, choroid, lens and iris. Due to its small thickness of 0.1 mm at the equator of the eye, the retina is not considered as an independent body in the eye model, but geometrically added to the choroid. The aqueous and vitreous are suppressed for the simulation. The volume of aqueous and vitreous is represented by hydrostatic fluid elements (HSFLD). When creating the geometry, attention is already paid to the spatial discretizability of the geometry in the FEM program and, for example, tapered edges are avoided for all expected adjustments. In order to allow for easy adaptation of the eye model to parameter combinations of real human eyes determined with ophthalmic devices, predefined dimensions of the design sketch are named after their medical equivalent and function as input parameters. All other measures and constraints within the sketch, that are not commonly measured by ophthalmic devices depend on the input parameters or have been set according to mean values from medical literature.

The input parameters that are adaptable out of the FEM software are: axial length (l), equator diameter, central corneal thickness (d), peripheral corneal thickness, corneal curvature radius, lens diameter and thickness, see Fig. 3. With these adjustable parameters all physiologically possible eye forms are covered.

Table 1 shows the default values that correspond to the mean value for each parameter in column 1. Columns 2 and 3 show the constructive boundaries at which the construction produces errors, e.g. intersections of two or more eye components or radial discontinuities of the fixed parameters. Additionally the extremal values from a clinical trial with $N = 96$ participants and the literature values of the biometric eye parameters are listed in columns 4–7. Note that not all parameters could be determined with the ophthalmic devices in the clinical trial. Concerning the constructive boundaries of the eye model, note that all eyes of the clinical trial series that was conducted to test the tonometer approach on humans could be reproduced.

2.1.2. Material parameters

In addition to the design of the eye geometry, an adequate description of the material properties is required for the FEM simulation. Due to the transient simulation to be carried out, which already requires a great amount of calculation effort, a simplification of the material properties with an isotropic linear-elastic material model is selected where applicable. The linear-elastic material model is defined by the Young's modulus, Poisson's ratio and density from [29,32], see Table 2. Cornea, sclera and iris that have nonlinear hyperelastic material features are represented as second order Ogden model [33–35]. All bodies of the eye consist mainly of water, whereby the density is close to 1 g/cm^3. Aqueous humor and vitreous are considered incompressible. The two fluid bodys are implemented as HSFLD. This implementation allows for a suppression of the aqueous humor and the vitreous body so that no elements are required which saves a large amount of computation effort.

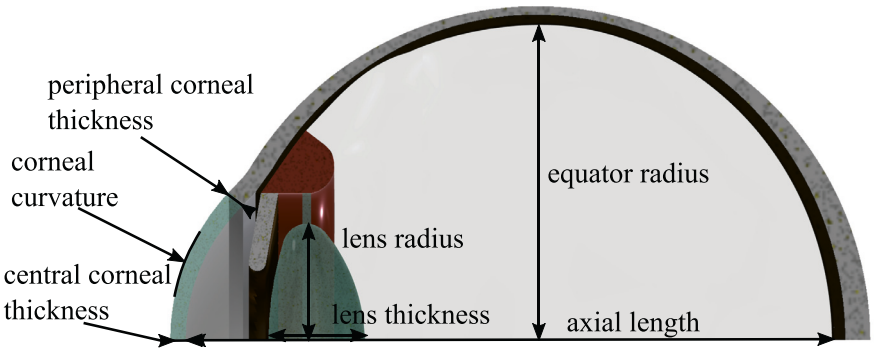

Fig. 3. Adjustable geometric input parameters of the CAD eye model.

Table 1
Adaptability of the parametric eye model with default values, constructive boundaries and literature values for the biometric eye parameters in human as well as determined extremal values from a clinical trial series. All values are in mm.

Input value	Default mean	Construction		Clinical trial		Literature	
		min	max	min	max	min	max
axial length	24	18	40	20.7	33.3	22	25
equator diameter	25	16	30	–	–	22	26
central corneal thickness	0.55	0.1	1.5	0.46	0.66	0.5	0.67
peripheral corneal thickness	0.67	0.4	1	–	–	0.67	0.7
corneal radius	7.8	7	10	7.2	9.3	7	8
lens diameter	7	5	9.2	–	–	6.5	9
lens thickness	4	3	7	–	–	3.5	6.5

Table 2
Material parameters of the eye model.

Eye body	Material modell / parameter	Density g/cm^3	Reference
	Hyperelastic Ogden 2nd order		
Iris	$\mu_1 = 0.0861$ MPa; $\alpha_1 = 54.255$; $\mu_2 = 0.0754$ MPa; $\alpha_2 = 48.072$	1.100	[34]
Cornea	$\mu_1 = 30$ Pa; $\alpha_1 = 140$; $\mu_2 = 2700$ Pa; $\alpha_2 = 105$	1.143	adjusted from [33]
Sclera	$\mu_1 = \mu_2 = 1439.7$ Pa; $\alpha_1 = 351$ $\alpha_2 = 500$	1.243	approximated [35]
	Linear elastic		
Lens	$E = 6.88$ MPa; $\nu = 0.47$	1.078	[29]
Reticular and choroidal skin	$E = 0.6$ MPa; $\nu = 0.49$	1.002	[36]
Ziliar body	$E = 11$ MPa; $\nu = 0.4$	1.600	[32]
Zonula fibers	$E = 358$ MPa; $\nu = 0.4$	1.000	[32]
	Hydrostatic Fluid Elements		
Aqueous humor	$K = 2$ GPa;	1.006	
Vitreous	$K = 2$ GPa;	0.95	

2.1.3. Boundary conditions

The FEM simulation of the eye is performed according to the boundary conditions at which the laboratory measurements are carried out to allow for comparability in terms of a model validation. This means that only the isolated eyeball is considered, i.e. without the surrounding fat tissue, muscles and eyelids. Similar to the laboratory tests (see Section 2.3), a ring-shaped fixed bearing can be assumed for the eye, that represents the circular opening of the pressure chamber, which the eye is placed on. In addition, the excitation pulse is applied to the eye in the form of a time-dependent pressure load. The template for this is the microphone recording from the inside of the pressure chamber from laboratory measurements on porcine eyes, shown as excitation in Fig 7. The third boundary condition is the IOP to be measured within the eye. The IOP is put up by the HSFLD, that simulate a constant pressure of an incompressible fluid. The eye is simplified to be rotationally symmetrical around the x-axis, because the boundary conditions are also rotationally symmetrical, see Fig. 4.

For this analysis it is neglected that the cornea has a slightly elliptical shape. The overall amount of mesh cells can be reduced by 75% by symmetry planes which allows a finer spatial discretization for the 3D FEM model, which provides more reliable results without overbid the calculation effort. Fig. 5 shows the mesh used for the simulation. A mesh study was performed, which shows that a halving of the used mesh dimensions results in a variation of 0.1 µm for calculated corneal deflections. The dimension settings for the mesh were identical in all simulations.

Since the eye bodies are defined as an assembly, ANSYS sees all eye bodies as bonded, without further contact definitions.

The transient calculation simulates a period of 20 ms, which is sufficient to obtain the corneal deflection amplitude that is currently used to trace back to the IOP. The settling process required to apply the IOP to the geometry is calculated without time integration as an individual load step, to avoid dynamic effects of the

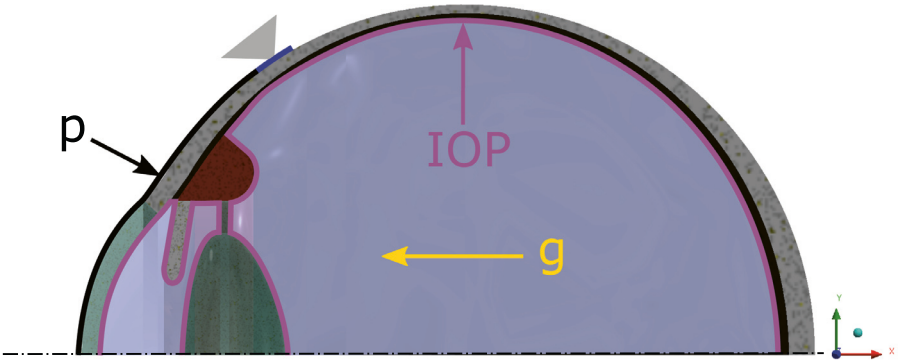

Fig. 4. Boundary conditions of the simulation: excitation pressure p, gravity g, a fixed bearing and the IOP. The liquid bodies of the eye are represented by hydrostatic fluid elements (HSFLD). The eye model is symmetrical along the x-axis.

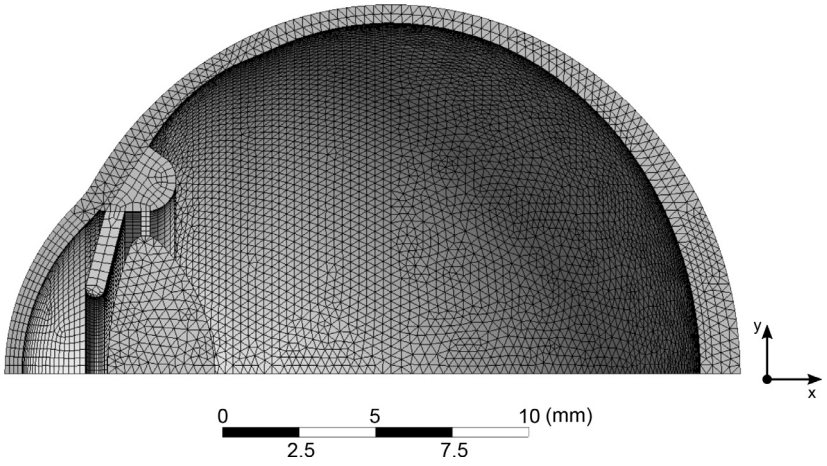

Fig. 5. Mesh used for the calculation.

IOP initialization. The minimal time step is 1 µs. The point on the axis of rotation on the outside of the cornea, which corresponds to the apex position, is stored over all time steps and used for the subsequent evaluation and comparison to the laboratory measurements. The corneal deflection amplitude A, that is finally obtained, is a function of the desired IOP (measured) and biometric eye parameters BEP:

$$A = f(IOP, BEP). \tag{1}$$

2.2. Use of the parametric eye model to define systematic relations to BEP

In order to quantify the influence of two sample BEP on the measurement uncertainty, which can be captured by the ophthalmologist and be included in IOP determination, the axial length l and the central corneal thickness d of the eye are used as a sample application. By the use of Gaussian error propagation [37], the quantitative influence on the measurement uncertainty of the measurement principle can be determined:

$$u(IOP) = \left|\frac{\partial IOP}{\partial A}\right| \cdot \sqrt{u_A^2 + \left(\frac{\partial A}{\partial l}\right)^2 \cdot u_l^2 + \left(\frac{\partial A}{\partial d}\right)^2 \cdot u_d^2}. \tag{2}$$

The sensitivity $\frac{\partial A}{\partial IOP}$ of the measuring principle that is obtained from experimental results is inverted and forms the basis of the uncertainty propagation calculation, where A describes the amplitude of excited corneal deflections and IOP the prevalent intraocular pressure. The standard deviation u_A describes the random deviations caused by the measuring system and is obtained from repeated laboratory measurements. The standard uncertainties u_l and u_d describe the natural variation of biometric eye parameters and are estimated from a clinical trial series. The mean value of the eye length $\bar{l} = 24$ mm and the standard deviation $s(l) = 1.8$ mm and also the central corneal thickness $\bar{d} = 545$ µm and an empirical standard deviation $s(d) = 37$ µm were calculated from the data set of the clinical trial series. Thus for the calculation of Eq. (2) $u_l = 1.8$ mm and $u_d = 37$ µm are used. When one parameter is varied, all other adjustable parameters are set to the mean value of a human eye stated in Table 1. The IOP is set to 15 mmHg, which corresponds to the physiological normal pressure in humans [4]. The eye model allows to define the relations $\frac{\partial A}{\partial l}$ and $\frac{\partial A}{\partial d}$ for the observed range of the clinical trial series and hereby completes Eq. (2).

2.3. Validation measurements

In order to quantify the deviations between eye model predictions and real measurements further laboratory tests on porcine eyes are conducted similar to [20], whereby this time the eye geometry is measured with a caliper.

2.3.1. Setup for porcine eye measurements

The laboratory measurements are carried out with porcine eyes of animals 6 to 8 months old, which are a by-product from industrial slaughtering. The biomechanical properties of porcine eyes are very similar to those of human eyes and their use in laboratory tests is ethically preferred. The porcine eyes are stored immediately after slaughter in 0.9% isotonic saline solution at room

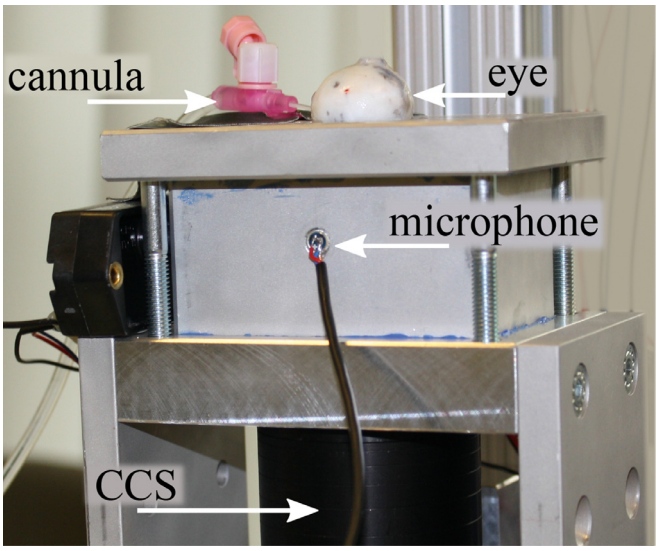

Fig. 6. Setup for porcine eye measurements. The confocal chromatic sensor (CCS) detects the corneal deflection within the pressure chamber through an optical window.

temperature (20 °C). This prevents the enucleated eyes from desiccation, so that in vivo-like properties are present during the measurement. For the laboratory measurements, the eyes are cleansed of the attached muscular and fat tissue and placed on the measurement setup with the cornea facing to the inside of the pressure chamber, see Fig. 6. The focus point of the used confocal chromatic sensor (CCS) (*IFS2405-10, Micro-Epsilon*) with a diameter of 16 µm is located in the center of the cornea (apex). The IOP is adjusted by a liquid column from 5 to 40 mmHg via a cannula connected to the eye, so that the influence of the IOP on the corneal oscillation can be investigated. In laboratory measurements, the corneal amplitude within the pressure chamber is measured by the CCS through an optical window in the bottom of the pressure chamber. The spatial resolution of the CCS is 60 nm and the measurement range is 10 mm, which allows to acquire the expected range of corneal deflection. The occurring oscillation frequencies to about 1 kHz are sampled with 10 kHz by the CCS.

3. Results

3.1. Results of validation measurements

Eight porcine eyes have been tested at adjusted IOP levels from 5 to 40 mmHg. The recorded oscillations for a sample eye are displayed in Fig. 7. In Fig. 7 two significant changes in the oscillation characteristic resulting from the IOP level are observed. First the positive amplitude of the corneal deflection decreases at rising IOP levels. Second the temporal distance between the excitation and the first maximal value decreases at rising IOP levels, which results in a frequency increase with rising IOP values. From 30 mmHg the frequency then decreases again which shows an ambiguity in the IOP dependent frequency change.

The IOP-dependent functional value that is used throughout this analysis is the first maximum of the corneal deflection, the amplitude A. In Fig. 8 the peak values of the amplitudes from Fig. 7 are plotted against the prevalent IOP values together with the simulation results. The dimensions of the simulated eye are adapted to the caliper measured dimension of the presented porcine eye. For the comparison $l = 19.9$ mm and $d = 900$ µm were used. The equator diameter amounts to 22 mm.

The corneal deflection decreases when the IOP is raised in simulation and measurements. The function of IOP can be expressed by Eq. (3) for an exponential decay:

$$f(x) = a \cdot e^{b \cdot x} + c, \quad a, b \text{ and } c \in \mathbb{R} \tag{3}$$

Both, the simulation results and the measured amplitude values show a similar trend for a change in IOP level, which indicates, that the measurement principle is covered by the simulation. The quantified deviations between measurement values and simulation results are below 8 µm at six IOP values. The eye model is considered validated due to the similar IOP-dependent behavior of and low deviation to the laboratory measurement.

3.2. Influence of axial length (l) on corneal deflection amplitude A

According to the clinical trial series the axial length (l) was varied in a range from 21 to 27 mm to cover 95 % of measured values symmetric to the mean. Since the eye is considered as a spherical object, l also changes the geometric relationships to the other parameters in the eye, e.g., to the equator diameter of the eye and thus also to the curvature of the sclera. In Fig. 9 is specified, how the amplitude A of corneal deflection changes over l according to the eye model from Section 2.1. The corneal deflection amplitude decreases with increasing l. This tendency seems reasonable, since the moment of inertia of the round structure increases with increasing l in the direction of loading and thus provides more resistance to deformation. The curve behavior can be described approximately with a 2^{nd} order polynomial. The relation between l and A is herewith determined by the eye model and can be used to solve Eq. (2).

3.3. Influence of the central corneal thickness (d) on corneal deflection amplitude A

The central corneal thickness d differs from person to person. In static IOP measurement, e.g. with the GAT, the thickness of the cornea plays an important role and is responsible for high measurement deviations if it is not taken into account, see Section 1. In the simulation, the oscillation amplitude of the cornea up to 0.65 mm becomes larger as d increases. This behavior does not seem physically plausible at first, since a thicker cornea mechanically applies more resistance to the pressure pulse and should therefore lead to smaller deformations. When observing the pre-expansion of the eye by the IOP, it is apparent that the cornea bulges outwards less with increasing thickness, see Fig 10b. The maximum difference in bulging is 25 µm from 0.4 to 0.7 mm. Due to the bulging, a change in the moment of inertia of the round structure in the direction of loading occurs, whereby the moment of inertia of the structure increases with a thinner cornea and decreases with a thicker cornea. This effect superimposes the corneal deflection according to the thickness and leads to a tenfold smaller change of 2.2 µm between 0.4 to 0.55 mm in Fig. 10a compared to the bulging.

3.4. Quantification of uncertainty contributions

With the provided relationship of the BEP to the corneal deflection amplitude of the eye model, the uncertainty contributions can now be determined. For the calculation with Eq. (2) $\frac{\partial IOP}{\partial A}$ was determined by the exponential fit of the laboratory measurements displayed in Fig. 7. $\frac{\partial A}{\partial l}$ and $\frac{\partial A}{\partial d}$ were taken from Figs. 9 and 10 a. In Fig. 11 the stochastic and systematic uncertainty contributions are plotted against the IOP.

The share of measurement uncertainty $u(IOP)_l$ caused by dispersion of the biometric parameter dominates the share by the stochastic measurement deviation of the confocal chromatic sensor $u(IOP)_{sto}$. The uncertainty contribution of the central corneal thickness is calculated smaller than stochastic contributions. As shown

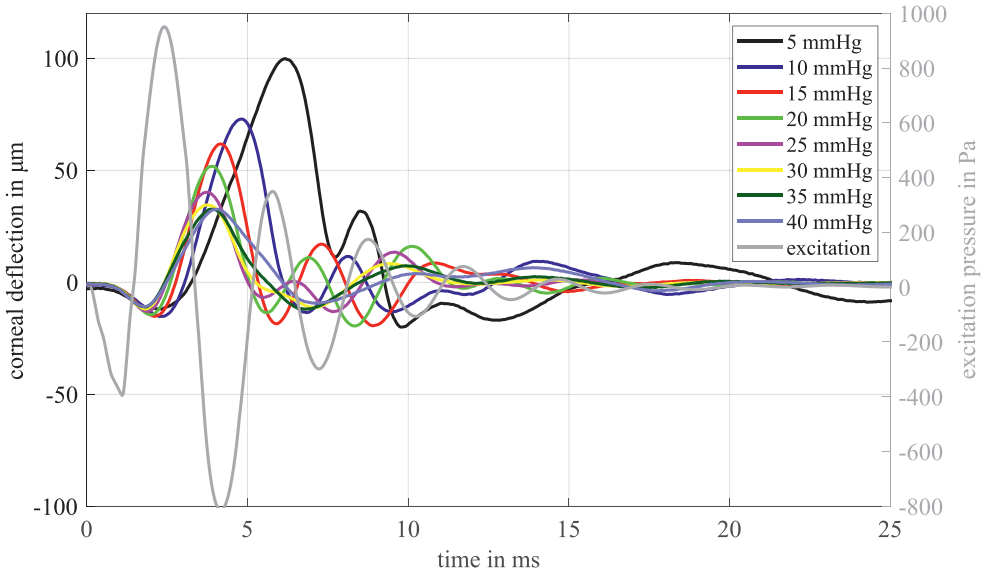

Fig. 7. Corneal deflection of a sample porcine eye measured with the CCS. With an increase of the IOP, the amplitudes of the oscillation decrease from 15 mmHg and the frequency rises.

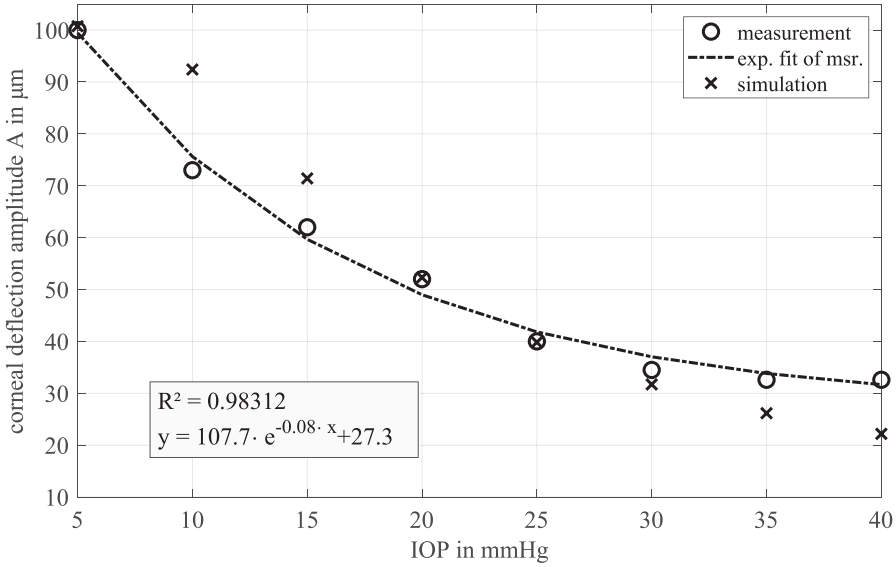

Fig. 8. Corneal deflection amplitude *A* in laboratory measurements and simulation with a fit of the laboratory values according to Eq. (3). The agreement between simulation and measurement is below 8 µm for 5 mmHg and from 15 to 35 mmHg, which shows the conformity in the tendential course.

in Fig 10b its influence on the measured relative corneal deflection is superimposed by the tenfold larger influence of the pre-expansion of the cornea caused by the IOP. If only the stochastic influences during measurement are considered, a measurement uncertainty of < 2.3 mmHg over the complete measurement range can be achieved. If the influence of l remains uncorrected, the achievable uncertainty of measurement is between 0.5 mmHg (at IOP $= 5$ mmHg) and 7.5 mmHg (at IOP $= 40$ mmHg). This proves the significant influence of the BEP l on the IOP measurement and is a first attempt to quantify this influence depending on the BEP using the adaptive FEM eye model.

4. Discussion

An adaptive eye model was created to investigate systematic influences resulting from variations of biometric eye parameters (BEP) on an acoustic tonometry approach. The adaptive eye model provides the functionality to simulate all eye shapes of participants of a clinical trial series. The performed simulations quantify the influence of two sample BEP (l and d) of the eye on the measurement uncertainty of the acoustic self-tonometer. Consequently, BEP must be taken into account in the measurement in order to correct the expected systematic measurement errors in different patients. The adaptive eye model provides the relations between the BEP and the corneal deflection amplitude A. By supplementary measuring the BEP along with the tonometry measurement, the systematic deviation resulting from cross-sensitivities are reduced. The central corneal thickness was found to play a minor role compared to the GAT as its effect is superimposed by a pre-expansion of the cornea that results in a change of moment of inertia in the direction of the load.

The use of hydrostatic fluid elements in ANSYS solved the problem of an adequate boundary condition for the pressurized liquid bodies inside the eye and saved a major amount of computation effort. However, by using this abstraction, the time resolved wave propagation throughout the liquid eye bodies was neglected.

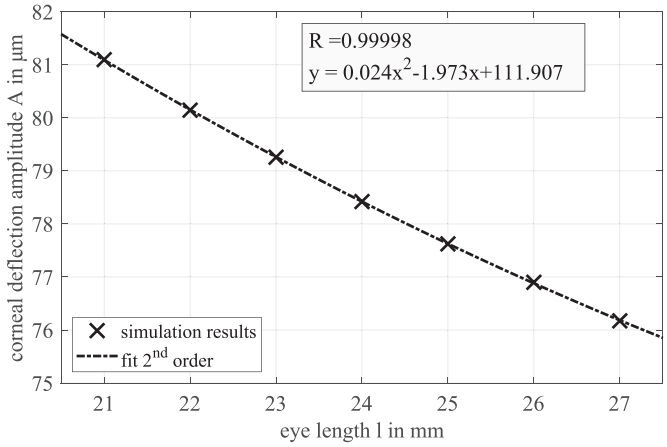

Fig. 9. The corneal deflection amplitude *A* calculated from the FEM simulation plotted over the axial length *l*. The simulation results were approximated with a 2nd order polynomial. With increasing *l* *A* decreases.

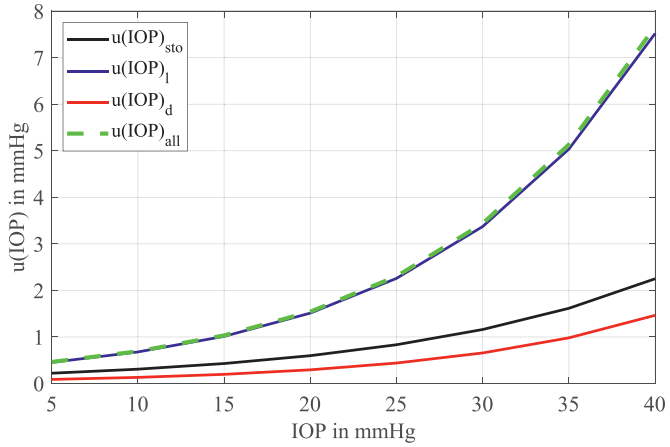

Fig. 11. The calculated measurement uncertainty as a function of the IOP for stochastic $u(IOP)_{sto}$ and systematic $u(IOP)_l$, $u(IOP)_d$ contributions. The uncertainty contribution of the axial length *l* clearly dominates the stochastic influences. The uncertainty contribution of the corneal thickness is comparably small.

For the simulation of corneal deformations in noncontact tonometry, Ariza-Gracia et al. [38] suggested a fluid-structure interaction (FSI) simulation to consider the liquid eye bodies as fluid to receive most realistic deformation behavior. Montanino et al. [39] focused on the interaction formulation of fluid and solid in order to improve the temporal deformation behavior of the cornea in a simplified model of the anterior segment of the eye and achieved results in good agreement to the temporal deformations observed by *Corvis ST* measurements. The findings by Ariza-Gracia et al. [38] and Montanino et al. [39] could help to improve the temporal behavior of the FEM eye model and may explain the persistent deviation compared to laboratory tests. However, implementing a FSI simulation in the parametric FEM eye model would have set another challenging focus on the investigation, which has been held back for now. Also the use of a viscoelastic material model to describe the time dependent behavior of the vitreous is planned to be implemented, since the vitreous describes a major share of the eye's volume. However, due to the low deformation, it is not expected that a change in the dependencies determined in this paper on the adaptation of BEP will occur. The adaptive eye model so far represents the validated IOP-dependent decrease in corneal deflection amplitude and thus provides the basis of a model assisted measurement approach.

Compared to other eye models that can be found in literature [27,29–33,38,40] there was no work found that has the cutting quantity of a geometrically adaptable eye model and the validated IOP-dependent behavior for the acoustic tonometry approach described by [19].

The laboratory measurements agree with the expectation from previous studies [20]. It was explained in Osmers et al. [19], that the eye puts up more resistance to deformation with increasing IOP values, which results in smaller corneal deflections. Compared to the eye models behavior the evaluated corneal deflection amplitude especially differs for the low IOP value of 10 mmHg from the amplitudes of the laboratory measurement. It is assumed, that the corneal oscillation behavior changes, when the IOP is below 15 mmHg in a highly nonlinear manner. This may lead to anisotropic buckling of the cornea that cannot be covered by the simplified eye model. On the measurement side it was noticed, that difficulties to measure exactly in the apex position sometimes occur for low IOP values. The inflation of the eye mainly changes the shape of the cornea for low IOP values below 15 mmHg. In order to reach a sufficient signal-to-noise ratio for the confocal chromatic sensor, a repositioning of the eye is required if the inflation causes a deviation of the focal point of the sensor to the apex position of the cornea. The model predicted change of measured corneal deflection amounts to 30% with a distance of 3 mm to the apex position. In order to improve the consistency of model and experiment, a camera assisted positioning procedure can be used to reduce the positioning uncertainty and assure the oscillation detection in the apex position throughout all IOP levels.

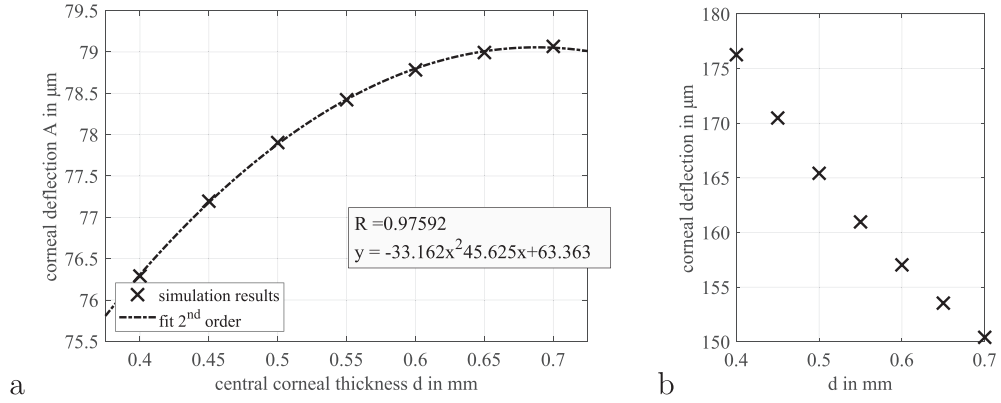

Fig. 10. (a) The corneal deflection amplitude *A* calculated from the FEM simulation plotted over the central corneal thickness *d*. The simulation results were approximated with a 2nd order polynomial. (b) The pre-expansion of the cornea due to the constant IOP of 15 mmHg. A thinner cornea leads to a larger pre-expansion.

Since the material parameters for biological tissue differ greatly among the variety of literature sources [28,29,32,33,41,42], it could lead to a better agreement between simulation and measurement, if the material parameters are acquired directly for the measured porcine eyes. This might explain the deviations even though the geometry was kept the same. The eye model provides a tool that can be adapted geometrically and would be improved further by the use of in vivo determined material models.

5. Conclusion and outlook

In order to analyze the influence of the biometric eye parameters on the accuracy of an acoustic self-tonometer, an adaptive eye model was created that covers all physiological shapes of the human eye. The IOP dependent behavior of the eye model is validated by laboratory measurements with enucleated porcine eyes. Systematic influences of the axial length l and the central corneal thickness d on the measurement principle were then analyzed using the adaptive FEM eye model, which provides the required relation of biometric parameters to the corneal deflection amplitude A (output quantity of the acoustic self-tonometer). The cross-sensitivities were quantified in the simulation and combined with the laboratory measurements via a Gaussian uncertainty propagation. Using the data set of a clinical trial series, the empirical standard deviation for the axial length of the eye (1.8 mm) and the central corneal thickness (37 µm) are used as a measure of the expected fluctuations during measurements with the self-tonometer. This results in a maximum systematic uncertainty contribution of 7.5 mmHg for l and 1.5 mmHg for d (extended uncertainty of measurement $k_p = 2$), whereas the stochastically conditioned amount with maximum 2.3 mmHg is comparably small. A correction of the influence of the axial length is therefore necessary to reduce the measurement uncertainty to below 5 mmHg at prevalent IOP values up to 40 mmHg.

The following research activities will focus on the analysis of further biometric eye parameters and investigate the influences of the eye environment during in vivo measurements. Furthermore the influence of wave propagation and viscoelasticity is planned to be investigated. The adaptive eye model can already be used for systematic investigation of biometric influences on the measurement process and allows for better understanding and a possible compensation of systematic uncertainty contributions.

Declaration of Competing Interest

Authors declare that they have no conflicts of interest.

Acknowledgements

The results in this journal article have been achieved within the project “SelTon-X”. The project was funded by the German Federal Ministry for Economic Affairs and Energy (BMWi, reference number 03THW04H02).

References

[1] S. P. Mariotti, Global data on visual impairements 2010, 2012, URL: http://www.who.int/blindness/GLOBALDATAFINALforweb.pdf (accessed: 31.07.2019), (Sep.).
[2] J.B. Jonas, T. Aung, R.R. Bourne, A.M. Bron, R. Ritch, S. Panda-Jonas, Glaucoma, Lancet 390 (10108) (2017) 2183–2193.
[3] E.M. Hoffmann, L.M. Zangwill, J.G. Crowston, R.N. Weinreb, Optic disk size and glaucoma, Surv. Ophthalmol. 52 (1) (2007) 32–49, doi:10.1016/j.survophthal.2006.10.002.
[4] F. Grehn, Augenheilkunde, Springer, Berlin Heidelberg, 2008.
[5] T. Huseynova, G.O. Waring, C. Roberts, R.R. Krueger, M. Tomita, Corneal biomechanics as a function of intraocular pressure and pachymetry by dynamic infrared signal and scheimpflug imaging analysis in normal eyes, Am. J. Ophthalmol. 157 (4) (2014) 885–893, doi:10.1016/j.ajo.2013.12.024.
[6] P.A. Tonnu, T. Ho, T. Newson, A.E. Sheikh, K. Sharma, E. White, C. Bunce, D. Garway-Heath, The influence of central corneal thickness and age on intraocular pressure measured by pneumotonometry, non-contact tonometry, the tono-pen xl, and Goldmann applanation tonometry, Br. J. Ophthalmol. 89 (7) (2005) 851–854.
[7] H. Goldmann, T.H. Schmidt, Applanation tonometry, Ophthalmologica 134 (4) (1957) 221–242.
[8] M. Kohlhaas, A.G. Boehm, E. Spoerl, A. Pürsten, H.J. Grein, L.E. Pillunat, Effect of central corneal thickness, corneal curvature, and axial length on applanation tonometry, Arch. Ophthalmol. 124 (4) (2006) 471–476, doi:10.1001/archopht.124.4.471.
[9] A. Mehdizadeh, A. Hoseinzadeh, A. Fazelzadeh, Central corneal thickness as a risk factor for glaucoma, Med. Hypotheses 69 (6) (2007) 1205–1207, doi:10.1016/j.mehy.2006.12.066.
[10] J. Wachtl, M. Töteberg-Harms, S. Frimmel, C. Kniestedt, Evaluation von korrekturformeln für die tonometrie, Der Ophthalmol. 114 (8) (2016) 716–721, doi:10.1007/s00347-016-0409-3.
[11] J.D. Brandt, J.A. Beiser, M.A. Kass, M.O. Gordon, Central corneal thickness in the ocular hypertension treatment study (OHTS), Ophthalmology 108 (10) (2001) 1779–1788, doi:10.1016/s0161-6420(01)00760-6.
[12] K. Sapkota, S. Franco, M. Lira, Intraocular pressure measurement with ocular response analyzer over soft contact lens, Contact Lens Anterior Eye 37 (6) (2014) 415–419, doi:10.1016/j.clae.2014.07.002.
[13] D.A. Luce, Determining in vivo biomechanical properties of the cornea with an ocular response analyzer, J. Cataract. Refract. Surg. 31 (1) (2005) 156–162, doi:10.1016/j.jcrs.2004.10.044.
[14] J.A. Cook, A.P. Botello, A. Elders, A.F. Ali, A. Azuara-Blanco, C. Fraser, K. McCormack, J.M. Burr, Systematic review of the agreement of tonometers with Goldmann applanation tonometry, Ophthalmology 119 (8) (2012) 1552–1557.
[15] A.A. Joda, M.M.S. Shervin, D. Kook, A. Elsheikh, Development and validation of a correction equation for corvis tonometry, Comput. Methods Biomech. Biomed. Eng. 19 (9) (2015) 943–953, doi:10.1080/10255842.2015.1077515.
[16] M. Matsuura, H. Murata, Y. Fujino, M. Yanagisawa, Y. Nakao, S. Nakakura, Y. Kiuchi, R. Asaoka, Repeatability of the novel intraocular pressure measurement from corvis ST, Transl. Vis. Sci. Technol. 8 (3) (2019) 48, doi:10.1167/tvst.8.3.48.
[17] A. Briceño, D. Mas, B. Doménech, Dynamic contour tonometry vs. non-contact tonometry and their relation with corneal thickness, Optik 127 (8) (2016) 3912–3917, doi:10.1016/j.ijleo.2016.01.026.
[18] N. Ehlers, T. Bramsen, S. Sperling, Applanation tonometry and central corneal thickness, Acta Ophthalmol. 53 (1) (1975) 34–43, doi:10.1111/j.1755-3768.1975.tb01135.x.
[19] J. Osmers, Á. Patzkó, O. Hoppe, M. Sorg, A. von Freyberg, A. Fischer, The influence of intraocular pressure on the damping of a coupled speaker-air-eye system, J. Sens. Sens. Syst. 7 (1) (2018) 123–130, doi:10.5194/jsss-7-123-2018.
[20] J. Osmers, M. Sorg, A. Fischer, Optical measurement of the corneal oscillation for the determination of the intraocular pressure, Biomed. Eng./Biomed. Tech. 64 (4) (2019) 471–480, doi:10.1515/bmt-2018-0093.
[21] L. Coquart, C. Depeursinge, A. Curnier, R. Ohayon, A fluid-structure interaction problem in biomechanics: prestressed vibrations of the eye by the finite element method, J. Biomech. 25 (10) (1992) 1105–1118.
[22] J. Drescher, Bestimmung des Intraoculardrucks aus dem Schwingungsverhalten des Humanauges, Universität Fridericiana Karlsruhe, 2000 Ph.D. thesis.
[23] S. Salimi, S.S. Park, T. Freiheit, Dynamic response of intraocular pressure and biomechanical effects of the eye considering fluid-structure interaction, J. Biomech. Eng. 133 (9) (2011) 091009, doi:10.1115/1.4005166.
[24] T.M. Nejad, C. Foster, D. Gongal, Finite element modelling of cornea mechanics: a review, Arq. Bras. Oftalmol. 77 (1) (2014) 60–65.
[25] T.D. Nguyen, B.L. Boyce, An inverse finite element method for determining the anisotropic properties of the cornea, Biomech. Model. Mechanobiol. 10 (3) (2011) 323–337, doi:10.1007/s10237-010-0237-3.
[26] A. Pandolfi, G.A. Holzapfel, Three-dimensional modeling and computational analysis of the human cornea considering distributed collagen fibril orientations, J. Biomech. Eng. 130 (6) (2008) 061006, doi:10.1115/1.2982251.
[27] P.M. Pinsky, D. van der Heide, D. Chernyak, Computational modeling of mechanical anisotropy in the cornea and sclera, J. Cataract Refract. Surg. 31 (1) (2005) 136–145, doi:10.1016/j.jcrs.2004.10.048.
[28] M.A. Lago, M.J. Rupèrez, F. Martínez-Martínez, C. Monserrat, E. Larra, J.L. Güell, C. Peris-Martínez, A new methodology for the in vivo estimation of the elastic constants that characterize the patient-specific biomechanical behavior of the human cornea, J. Biomech. 48 (1) (2015) 38–43, doi:10.1016/j.jbiomech.2014.11.009.
[29] A. Karimi, R. Razaghi, M. Navidbakhsh, T. Sera, S. Kudo, Computing the stresses and deformations of the human eye components due to a high explosive detonation using fluid–structure interaction model, Injury 47 (5) (2016) 1042–1050, doi:10.1016/j.injury.2016.01.030.
[30] A. Karimi, R. Razaghi, M. Navidbakhsh, T. Sera, S. Kudo, Quantifying the injury of the human eye components due to tennis ball impact using a computational fluid–structure interaction model, Sports Eng. 19 (2) (2016) 105–115, doi:10.1007/s12283-015-0192-4.
[31] A. Karimi, R. Razaghi, M. Navidbakhsh, T. Sera, S. Kudo, Computing the influences of different intraocular pressures on the human eye components using computational fluid-structure interaction model, Technol. Health Care 25 (2) (2017) 285–297.
[32] X. Liu, L. Wang, C. Wang, J. Fan, S. Liu, Y. Fan, Prediction of globe rupture caused by primary blast: a finite element analysis, Comput. Methods Biomech. Biomed. Eng. 18 (9) (2014) 1024–1029, doi:10.1080/10255842.2013.869317.

[33] A. Elsheikh, D. Wang, Numerical modelling of corneal biomechanical behaviour, Comput. Methods Biomech. Biomed. Eng. 10 (2) (2007) 85–95, doi:10.1080/10255840600976013.
[34] K. Zhang, X. Qian, X. Mei, Z. Liu, An inverse method to determine the mechanical properties of the iris in vivo, BioMedical Eng. OnLine 13 (1) (2014) 66, doi:10.1186/1475-925x-13-66.
[35] A. Eilaghi, J.G. Flanagan, I. Tertinegg, C.A. Simmons, G.W. Brodland, C.R. Ethier, Biaxial mechanical testing of human sclera, J. Biomech. 43 (9) (2010) 1696–1701, doi:10.1016/j.jbiomech.2010.02.031.
[36] T.R. Friberg, J.W. Lace, A comparison of the elastic properties of human choroid and sclera, Exp. Eye Res. 47 (3) (1988) 429–436.
[37] JCGM100, Evaluation of measurement data–guide to the expression of uncertainty in measurement, 2008,
[38] M.Á. Ariza-Gracia, W. Wu, B. Calvo, M. Malvè, P. Büchler, J.F.R. Matas, Fluid–structure simulation of a general non-contact tonometry. a required complexity? Comput. Methods Appl. Mech. Eng. 340 (2018) 202–215, doi:10.1016/j.cma.2018.05.031.
[39] A. Montanino, M. Angelillo, A. Pandolfi, Modelling with a meshfree approach the cornea-aqueous humor interaction during the air puff test, J. Mech. Behav. Biomed. Mater. 77 (2018) 205–216, doi:10.1016/j.jmbbm.2017.05.042.
[40] X. Liu, L. Wang, C. Du, D. Li, Y. Fan, Mechanism of lens capsular rupture following blunt trauma: a finite element study, Comput. Methods Biomech. Biomed. Eng. 18 (8) (2014) 914–921, doi:10.1080/10255842.2014.975798.
[41] T.H. Kwon, J. Ghaboussi, D.A. Pecknold, Y.M.A. Hashash, Effect of cornea material stiffness on measured intraocular pressure, J. Biomech. 41 (8) (2008) 1707–1713, doi:10.1016/j.jbiomech.2008.03.004.
[42] M.Á. Ariza-Gracia, S. Redondo, D.P. Llorens, B. Calvo, J.F.R. Matas, A predictive tool for determining patient-specific mechanical properties of human corneal tissue, Comput. Methods Appl. Mech. Eng. 317 (2017) 226–247, doi:10.1016/j.cma.2016.12.013.